ACS NANO
Cite This: ACS Nano 2019, 13, 1223−1231
www.acsnano.org

ARTICLE

Suppression of Electrochemically Driven Phase Transitions in Nanostructured MoS_2 Pseudocapacitors Probed Using *Operando* X-ray Diffraction

John B. Cook,[†,⊥] Terri C. Lin,[†] Hyung-Seok Kim,[‡,#] Andrew Siordia,[‡,∥] Bruce S. Dunn,[‡] and Sarah H. Tolbert*[,†,‡,§]

[†]Department of Chemistry and Biochemistry, University of California Los Angeles, Los Angeles, California 90095, United States
[‡]Department of Materials Science and Engineering, University of California Los Angeles, Los Angeles, California 90095, United States
[§]The California NanoSystems Institute, University of California Los Angeles, Los Angeles, California 90095, United States

Supporting Information

ABSTRACT: Pseudocapacitors with nondiffusion-limited charge storage mechanisms allow for fast kinetics that exceed conventional battery materials. It has been demonstrated that nanostructuring conventional battery materials can induce pseudocapacitive behavior. In our previous study, we found that assemblies of metallic 1T MoS_2 nanocrystals show faster charge storage compared to the bulk material. Quantitative electrochemistry demonstrated that the current response is capacitive. In this work, we perform a series of *operando* X-ray diffraction studies upon electrochemical cycling to show that the high capacitive response of metallic 1T MoS_2 nanocrystals is due to suppression of the standard first-order phase transition. In bulk MoS_2, a phase transition between 1T and triclinic phases (Li_xMoS_2) is observed during lithiation and delithiation in both the galvanostatic traces (as distinctive plateaus) and the X-ray diffraction patterns with the appearance of the additional peaks. MoS_2 nanocrystal assemblies, on the other hand, show none of these features. We hypothesize that the reduced MoS_2 crystallite size suppresses the first-order phase transition and gives rise to solid solution-like behavior, potentially due to the unfavorable formation of nucleation sites in confined spaces. Overall, we find that nanostructuring MoS_2 suppresses the 1T-triclinic phase transition and shortens Li-ion diffusion path lengths, allowing MoS_2 nanocrystal assemblies to behave as nearly ideal pseudocapacitors.

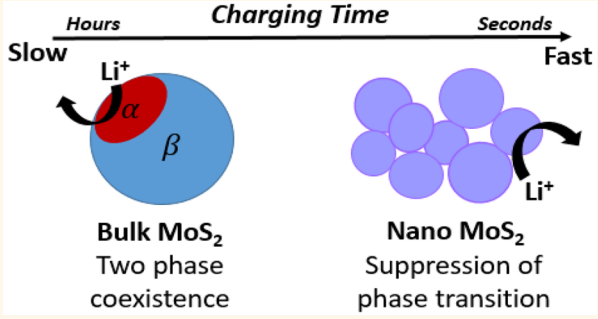

KEYWORDS: *MoS_2, phase transition suppression, pseudocapacitance, intercalation pseudocapacitor, fast charging, nanocrystal assemblies, porous electrodes*

Pseudocapacitance offers the potential for high power density (fast charging and discharging) without significant reduction in energy density. These values are typically highly anticorrelated in traditional Li-ion battery materials, and this decoupling of energy and power occurs by combining the storage mechanism of a battery and the kinetics more similar to an electric double layer capacitor (EDLC). Most battery materials have high energy density because the energy is stored through redox reactions in the bulk of the material. However, slow solid-state diffusion of the intercalating ions limits the kinetics of these reactions. EDLCs, on the other hand, store energy through the adsorption of ions onto high surface area electrodes, which produces fast kinetics, but sacrifices energy density.[1−5] Pseudocapacitive behavior commonly occurs when near-surface Faradaic charge transfer reactions take place, accompanied by ion adsorption electrochemically onto the host lattice in a process termed redox or surface pseudocapacitance. It can also occur, however, when ions intercalate into the channels or layers of a redox-active material, often near the surface of a material, without inducing a phase transition. This later process is called intercalation pseudocapacitance.[3−5]

Received: August 21, 2018
Accepted: December 31, 2018
Published: January 3, 2019

DOI: 10.1021/acsnano.8b06381
ACS Nano 2019, 13, 1223−1231

Typically, first-order phase transitions arise when there is a large variation in Li concentration during intercalation. This leads to the coexistence of Li-rich and Li-poor phases and results in a migration barrier that leads to slow kinetics observed in most intercalation materials.[6−8] The difference in volume of the two phases can also induce strain in the electrode, causing material failure and potentially reducing battery life.[7] Such phase transitions thus make traditional battery materials less attractive for fast charging applications.[3,4]

In keeping with the pseudocapacitor definition above, a number of materials that do not require a discontinuous phase transition for ion intercalation have been shown to exhibit pseudocapacitive behavior when diffusion path lengths are sufficiently reduced through nanostructuring to allow for fast ion diffusion into the bulk of the material. Such materials, which are known as intrinsic pseudocapacitors, include materials such as RuO_2,[9] MnO_2,[10,11] and Nb_2O_5.[4] Intrinsic pseudocapacitors have crystalline networks with ion transport pathways that allow for capacitive behavior and fast ion diffusion over a broad range of crystallite sizes.

Recently, it has been shown that pseudocapacitive behavior can also be achieved through suppression of first-order ion intercalation and deintercalation induced phase transitions.[1−4] Through nanostructuring, certain materials that do not display fast kinetics in the bulk can be engineered to become pseudocapacitive. These materials, termed extrinsic pseudocapacitors, are size dependent and do not show pseudocapacitive behavior above a critical size.[1,12] This phenomenon has been previously observed and shown in MoO_2,[12] TiO_2,[13−15] TiS_2,[16] and $LiMn_2O_4$.[17,18] When the diffusion path length shortens, rapid rates can be achieved because the diffusion time is proportional to the square of diffusion length and inversely proportional to diffusivity.[19] In addition, as the crystallite size decreases, two-phase coexistence (Li-rich and Li-poor) likely becomes undesirable, due to the increased activation energy for nucleation of the second phase or other thermodynamic or kinetic factors. This has the potential to again give rise to solid solution behavior, in which there is no miscibility gap and ions are interstitially dissolved into the lattice, causing only slight changes in the lattice parameter without major reconstruction of the crystal structure.[13,20,21]

Materials experiencing first-order phase transitions vs solid solution behavior show different features in their electrochemistry profiles, particularly in their galvanostatic (GV) traces. A voltage vs composition curve provides information on an electrode's thermodynamic properties such as the chemical potential, Gibbs free energy and entropy.[6,8] For systems with a miscibility gap in which Li-rich and -poor phases coexist, the chemical potential is derived using the common tangent construction of the Gibbs free energy minima of the two phases.[8] This results in distinctive plateaus in the voltage curve because the slope of the chemical potential is constant. As lithium intercalates and deintercalates into the host lattice of a pseudocapacitor without a phase transition, by contrast, the chemical potential of the active material is equal to the derivative of the Gibbs free energy and changes smoothly over the course of the electrochemical reaction. This leads to a linearly sloping voltage curve in the galvanostatic trace.[6,8] Thus, pseudocapacitive materials with solid solution-type behavior due to phase transition suppression do not show plateaus and can be easily differentiated from battery-like material with inherent first-order phase transitions.

Though pseudocapacitance has been demonstrated in several metal oxides, it has not been explored in many metal sulfides. Metal dichalcogenides are particularly interesting for their layered structure comprised of highly polarizable sulfur ions that allow reversible intercalation.[2,22,23] In the past, Muller *et al.* have demonstrated pseudocapacitive charge storage in few-layered 2D TiS_2 nanocrystals. In that study, 85% of the total current obtained from potentiostatic cycling was capacitive, leading to a high specific capacitance of 320 F/g with a 30 s charge/discharge time.[16] Recently, we have explored the pseudocapacitive properties of MoS_2 nanocrystals. MoS_2 is an attractive material for pseudocapacitive charge storage because of its relatively large van der Waals gap and electrochemically active metallic 1T phase. The 1T phase can be generated from the standard 2H phase by alkali metal intercalation.[22−26] Metallic materials are desirable in energy storage application due to their enhanced electronic conductivity. Details regarding the MoS_2 1T phase will be elaborated in the Results and Discussion section. In our previous study, we showed that thick electrodes made from MoS_2 nanocrystal arrays were pseudocapacitive. The electrodes could be cycled 3000 times with 80% capacity retention while accessing over 90 mA h g^{-1} in only 30 s (theoretical capacity 167 mAh g^{-1}).[27]

Despite MoS_2 being reported to undergo multiple phase changes to accommodate one mole of Li (167 $mAhg^{-1}$), these transitions appear to be suppressed in our MoS_2 nanocrystals arrays as evidenced by the high reversibility and fast kinetics.[27] In this work, we thus use *operando* X-ray diffraction during electrochemical cycling at the Stanford Synchrotron Radiation Lightsource (SSRL) to further understand the structural origin of the fast pseudocapacitive mechanism in MoS_2 nanocrystals. *Operando* X-ray diffraction has been shown to be an effective method for monitoring phase change and lattice expansion in energy storage materials in real time. It has been used to study materials such as $LiCoO_2$,[28] $LiMn_2O_4$,[29] $LiNiO_2$,[30] TiO_2,[14] and TiS_2.[20] This study provides a direct crystallographic comparison of micron-sized bulk MoS_2 ($bMoS_2$) and MoS_2 nanocrystal assemblies ($nMoS_2$) upon cycling with Li^+ with a goal of better understanding the drastic difference in performance between these two materials.

RESULTS AND DISCUSSION

Materials and Characterization. Bulk MoS_2 particles (~45 μm) used in this study are commercially available powders, while MoS_2 nanocrystals were synthesized according to methods in our previous work.[27] The powders were cast into composite slurry electrodes containing the active materials, carbon and polymeric binder. The synchrotron based X-ray diffraction patterns (XRD) of pristine $bMoS_2$ and $nMoS_2$ electrodes used in this *operando* study show characteristic reflections for the hexagonal MoS_2 phase matching JCPDS No. 37-1492 (Figure 1a). Since the XRD signal is attenuated by at least 50% due to absorption from various cell components and electrolyte, electrodes with relatively high mass loadings were made for this study. These electrodes were optimized in this study to produce a large XRD signal but could not be cycled at very high rates due to conductivity limitations. Any kinetic suppression of phase transitions that occurs at slow rates, however, should increase at faster rates, so the need to cycle slowly for these *operando* studies means only that these experiments represent a lower limit on the extent of phase transition suppression that could be observed at faster

DOI: 10.1021/acsnano.8b06381
ACS Nano 2019, 13, 1223−1231

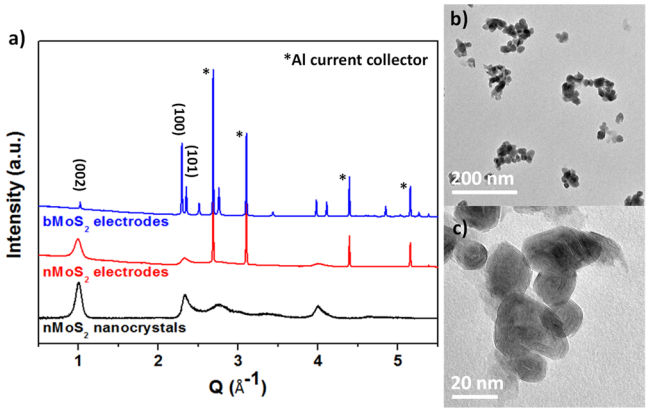

Figure 1. (a) XRD patterns of uncycled $bMoS_2$ and $nMoS_2$ electrodes and as-synthesized MoS_2 nanocrystals. Peaks labeled with an asterisk correspond to the aluminum current collector, while others correspond to the 2H phase of MoS_2. The peak broadening in the $nMoS_2$ electrode and pure nanocrystal sample is due to the small crystallite size and the onion-like structure of the 10 nm to 30 nm nanocrystals, as shown in the low (b) and high (c) magnification TEM images.

rates. Below we will show basically complete suppression, confirming that these scan rate differences do not modify our fundamental conclusions. In addition, the use of thick electrodes ensures that not all the $bMoS_2$ platelets settle parallel to the current collector, which would result in diminished peak intensities for the (00*l*) planes in the transmission geometry used in this work. The $nMoS_2$ nanocrystals (Figure 1b-c) are roughly spherical, leading to random orientation in the electrode. Indeed, the XRD patterns are consistent with a randomly dispersed polycrystalline MoS_2 powder. The average size of the $nMoS_2$ is 22 nm with a standard deviation of 7 nm. The histogram and the TEM images used to measure the $nMoS_2$ size can be found in Figures ESI 1 and 2.

Electrochemistry. MoS_2 has been studied as an energy storage material for decades. However, most current research focuses on the high capacity (670 mA h g^{-1}) conversion reaction which occurs between 1.1 and 0 V,[31−36] rather than the one electron intercalation reaction between 2.7 and 1.0 V. The cycle lifetimes for MoS_2 are typically poor for the conversion reaction even with engineered nanoparticle-based electrodes.[37] For the above reasons, we chose to focus on the intercalation reaction of MoS_2 between 2.7 and 1.0 V and have demonstrated high reversibility with our previous study.[23,27,38] The intercalation reaction can be described by eq 1:

$$MoS_2 + xLi^+ + xe^- \rightarrow Li_xMoS_2 \quad (1)$$

The 1T phase MoS_2 has been widely studied as a hydrogen storage material but has only recently been explored as an

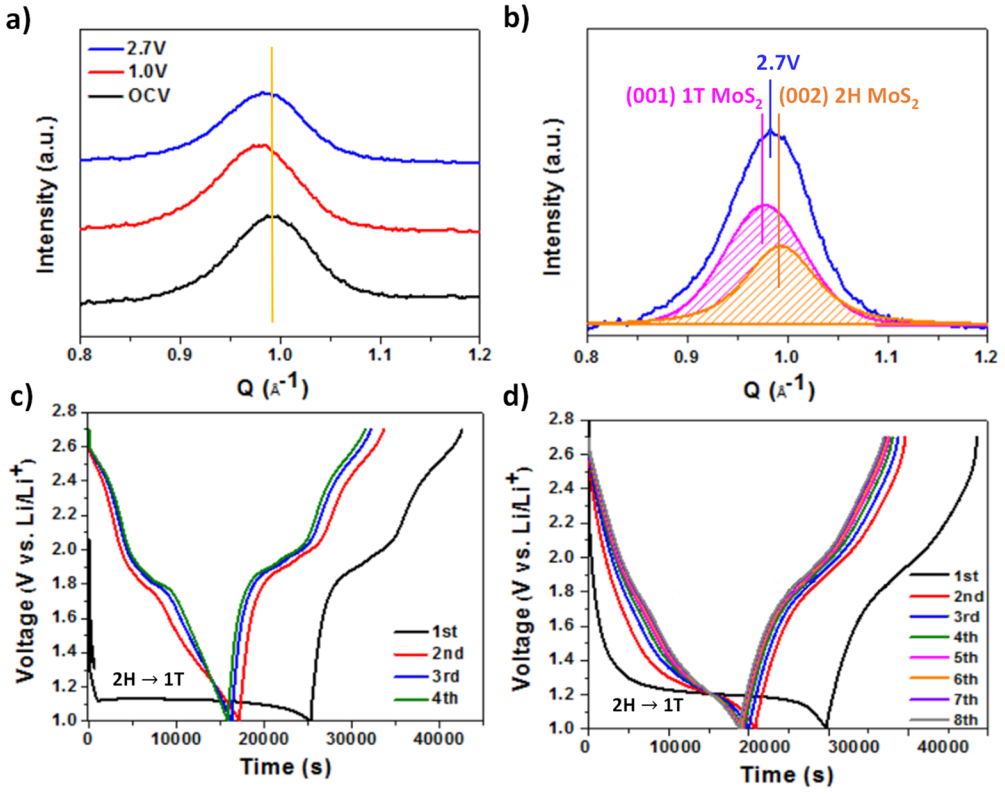

Figure 2. (a) *Operando* X-ray diffraction of $nMoS_2$ showing 2H to 1T conversion. Starting as the (002) 2H phase at the open circuit voltage, the 2H MoS_2 converts to the 1T phase during lithiation as the (002) 2H peak shifts to lower Q and becomes the (001) peak of the 1T phase. As lithium is deinserted, the (001) 1T peak shifts slightly back to higher Q, indicating the presence of both 1T and 2H phases since not all nanocrystals are converted in the first cycle. This mixture of two phases is confirmed by the peak fit analysis shown in (b), where the final peak position after delithiation lies in between the (001) 1T and (002) 2H phases. Parts (c) and (d) show galvanostatic profiles collected during the 2H to 1T conversion for bulk and nanosized MoS_2, respectively. Multiple cycles are required to complete the 2H-1T conversion, but the number of cycles is not the same for the two samples. Bulk MoS_2 (c) took 4 cycles, while nano MoS_2 (d) took up to 8 cycles. This precycling was done prior to the *operando* experiments presented below.

DOI: 10.1021/acsnano.8b06381
ACS Nano 2019, 13, 1223−1231

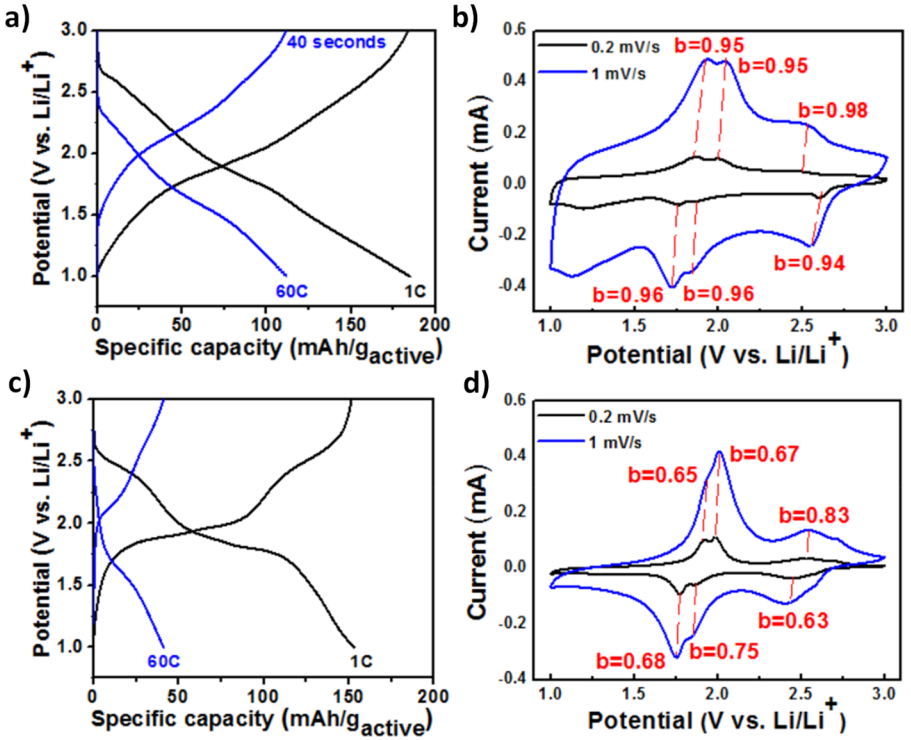

Figure 3. Galvanostatic traces and cyclic voltammograms of $nMoS_2$ (a-b) and $bMoS_2$ (c-d). The sloping galvanostatic profiles in (a) for $nMoS_2$ suggest that first-order phase transitions have been suppressed and that the system is pseudocapacitive. This is in agreement with calculated *b* values close to 1 at all the current maxima obtained from sweep rate dependent CV curves in (b); *b* = 1 indicates capacitor-like behavior. Unlike $nMoS_2$, phase transition between the 1T and triclinic $Li1MoS_2$ phases is indicated by voltage plateaus in $bMoS_2$ (c). The system also shows mostly diffusion-limited with *b* values close to 0.5 in (d).

energy storage material for pseudocapacitors.[39] The metallic 1T phase and the semiconducting 2H pristine phase are similar in structure, except 2H MoS_2 has a close-packed, layered hexagonal structure of S−Mo−S' in an ABA configuration, while 1T MoS_2 has an ABC configuration.[40−42] It is well-known that MoS_2 undergoes a phase conversion from 2H to 1T when alkali metals are inserted into the van der Waals gap, causing the highly polarizable sulfur layer to glide along the plane normal to the *c*-axis of the unit cell.[42−45] Lithium, in particular, causes an irreversible phase conversion from 2H to 1T (hexagonal to trigonal prismatic) at 1.1 V *vs* Li/Li^+ when the lithium concentration increases between the range of $0.1 < x < 1$.[43,46] Though the 2H to 1T phase conversion of $bMoS_2$ is well-known, it has not been directly observed in nanosized MoS_2. In addition to the *operando* phase change study of lithium intercalation within the 1T phase, we also performed *operando* X-ray diffraction to study the 2H to 1T phase conversion of $nMoS_2$ to help us better understand the conversion process and the 1T phase itself in $nMoS_2$.

The diffraction patterns of $nMoS_2$ during the first cycle are shown in Figure 2a in the pristine, lithiated (Li_1MoS_2) and delithiated states. The (002) peak shifts to a lower *Q* value ($Q = \frac{2\pi}{d}$) corresponding to the (001) peak of the 1T trigonal phase.[43,44,47] This same phenomenon has been observed in the bulk as 2H MoS_2 converts to 1T MoS_2 during alkali metal insertion. This peak shift is not simply a result of intercalation induced lattice expansion because the galvanostatic trace in Figure 2d shows a distinct plateau for this process that signifies a first-order phase transition. The peak broadening in this nanosized sample prohibited us from matching all high-order XRD reflections to the 1T phase, but a general matching is observed in Figure 1a. After delithiation, the (001) 1T peak shifted back to higher *Q*, to a value between the (001) 1T and (002) 2H peak positions, indicating that not all $nMoS_2$ in the electrode completed the 2H-1T conversion after the first cycle. Figure 2b shows the peak fit analysis of the delithiated $nMoS_2$ diffraction pattern, indicating the presence of both phases in the electrode.

Due to our interests in the fast intercalation reaction of MoS_2 in the 1T phase, all samples were precycled prior to *operando* diffraction studies to fully convert the semiconductinting 2H $bMoS_2$ and $nMoS_2$ to the metallic 1T phase *via* alkali metal intercalation. Figures 2c and d show the GV curves of $bMoS_2$ and $nMoS_2$, respectively, at 0.2 C during the course of the 2H to 1T conversion and precycling process. To ensure that most of the 2H phase is converted, $bMoS_2$ and $nMoS_2$ were precycled multiple times until the plateau at 1.1 V, corresponding to the 2H-1T conversion, completely disappeared. Moreover, it is known that 1T MoS_2 is not thermodynamically stable at high potential and can back convert to the 2H phase when cycled above 2.8 V vs Li/Li^+.[43,48] Therefore, all electrochemical cycling carried out in this study is limited to a voltage window of 1 to 2.7 V.

Interestingly, we found that, $bMoS_2$ took fewer cycles than $nMoS_2$ to complete the 2H to 1T conversion, as shown in the precycling GV traces in Figures 2c-d. The 2H $bMoS_2$ is completely converted to the 1T phase after four cycles, while $nMoS_2$ requires eight cycles. The longer conversion process for $nMoS_2$ foreshadows the results below and indicates different 2H to 1T phase transition kinetics in the nanoscale system compared to the bulk material. The conversion of 2H MoS_2 to the 1T phase is a first-order phase transition that is expected to

DOI: 10.1021/acsnano.8b06381
ACS Nano 2019, 13, 1223−1231

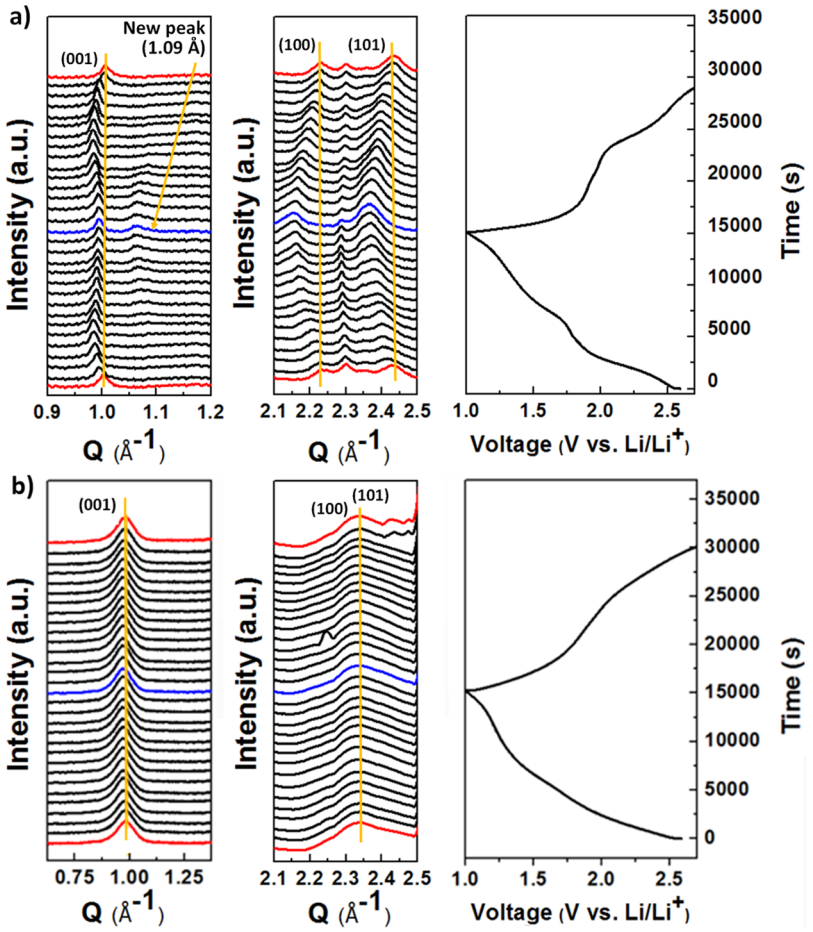

Figure 4. (a) *Operando* phase change study of $bMoS_2$ and $nMoS_2$. First-order phase transition can be observed in $bMoS_2$ as 1) peaks shift significantly to lower *Q* and then back to higher *Q*, 2) the emergence of an additional peak at 1.09 $Å^{-1}$, and 3) a shoulder near the 101 peak. (b) Unlike $bMoS_2$, no phase transition was observed in $nMoS_2$ due to the improved kinetics and unfavorable two phase coexistence in nanocrystals.

proceed *via* a nucleation and growth-type mechanism. The phase transition would thus require the formation of a 1T nucleus in the MoS_2 grain, followed by propagation or growth throughout the domain. The kinetics of phase transition could be more facile in the $bMoS_2$ for two reasons. First, nucleation may be suppressed in nanosized domains. Second, many more nucleation events are likely needed in the nanoscale material because of the limited domain volume transformed by each nucleation event.[49−52] Many microns of material can be transformed by a single nucleation event in the bulk, whereas every nanocrystal requires its own nucleation event. As a result, more cycles are required to propagate and complete the 2H-1T phase conversion in the $nMoS_2$ electrode. The peak positions for the $nMoS_2$ at OCV (2H phase) and at 2.7 V after multiple precycles (1T phase) are 0.990 Q and 0.979 Q, respectively.

Kinetics Analysis. Pseudocapacitive energy storage is a distinct electrochemical mechanism that gives rise to fast charge storage. As mentioned earlier in this manuscript, typical battery materials undergo distinct phase changes during lithium intercalation and deintercalation, and this type of charge storage is slow. In contrast, charge stored through intercalation pseudocapacitance does not result in phase transitions but instead is thought to occur through fast intercalation. Suppressing phase transitions permits fast intercalation reactions throughout the nanoparticle, enabling a pseudocapacitive charge storage mechanism that is not limited to the surface.

Pseudocapacitive storage gives rise to distinct electrochemical features in cyclic voltammogram (CV) and GV profiles. Specifically the sloping GV profiles discussed above should be accompanied by CV curves that show little polarization induced splitting between the anodic and cathodic peaks due to the fast kinetics and reduced crystallite size.[4] Figure 3a shows the GV curves at 1 and 60 C for $nMoS_2$, while panel b shows the CV curves collected at 0.2 mV/s and 1 mV/s for the same material. Though there are no plateaus observed in the $nMoS_2$ GV curves, redox peaks are present in the CV data, even at high rates. This suggests that the redox reactions are happening under suppression of phase transition, which is a characteristic of pseudocapacitive energy storage mechanism. Minimal peaks splitting is observed between anodic and cathodic peaks in Figure 3b. In comparison to $nMoS_2$, electrochemical traces of $bMoS_2$ show none of these features. Figures 3c and d show the GV and CV curves (same rates as the nanocrystals) for the bulk electrode. The distinctive plateaus in $bMoS_2$'s GV curve correspond to the phase transitions between the trigonal prismatic 1T phase and triclinic (Li_xMoS_2) phase during lithium intercalation.[48] Moreover, highly polarized redox peaks are observed in the CV as a result of the slower kinetics, indicating battery-like behavior in $bMoS_2$.

DOI: 10.1021/acsnano.8b06381
ACS Nano 2019, 13, 1223−1231

Kinetic analysis was performed to further understand the difference in behavior of $bMoS_2$ and $nMoS_2$ and to validate the pseudocapacitive behavior of $nMoS_2$ since sloping GV traces can also be triggered by the nanosize effect.[53] It has been observed that nanosize crystallites can lead to a sloping voltage curve due to a shorter voltage plateau width (*i.e.* a narrower two phase coexistence region) and can create solid solution-like electrochemical features, even when the first-order phase transition is not suppressed.[53]

To distinguish the type of charge storage process, "b-value" analysis was performed. This kinetic analysis has also been performed on many other pseudocapacitive materials such as Nb_2O_5,[4,54] V_2O_5,[55] and MoO_3.[21,56] Generally, the current response as a function of scan rate in a cyclic voltammetry measurement can be used to distinguish between a capacitor-like or diffusion controlled charge storage mechanism according to the following equation

$$i = av^b$$

where i is the measured current, v is the scan rate, and a and b are both constants, but the value of the exponential term distinguishes the charge storage mechanism: when b is equal to 0.5 (the current i is proportional to scan rate $v^{1/2}$), the current is dominantly governed by diffusion.[2,4] When b equals 1 (i is directly proportional to v), it indicates a capacitor-like behavior, where the current is not diffusion controlled, a situation that arises for surface pseudocapacitive reactions or when intercalation reaction kinetics is capacitive in nature due to the suppression in phase transitions.[2,4] According to our analysis shown in Figures 3b and d, $bMoS_2$ is found to be mostly diffusion-limited with b values at current maxima (0.65, 0.67, 0.68, 0.75) closer to 0.5. On the other hand, $nMoS_2$ is highly capacitive, with b values (0.95, 0.95, 0.96, 0.96) close to 1. The b-values with their corresponding peaks of $bMoS_2$ and $nMoS_2$ can be found in the CV in Figures 3b and d. This result suggests that $nMoS_2$'s sloping GV profile is due to phase transition suppression and not nanosize effect. Details regarding our analysis can be found in our previous studies on nanoscale MoS_2 and other nanoscale pseudocapacitors.[2,4]

Operando X-ray Diffraction Study. The structural changes occurring during Li^+ intercalation into 1T MoS_2 materials were observed using *operando* synchrotron X-ray diffraction. The diffraction patterns in Figures 4 and 5 were collected from $bMoS_2$ and $nMoS_2$ electrodes, respectively, that were precycled several times to drive the 2H-1T conversion. To reiterate, we are not studying the semiconductor to metal phase transformation. We are studying the phase stability of the metallic 1T phase during charge storage to understand the origins of fast charge storage in $nMoS_2$. Any resulting changes in the atomic structure of the host lattice will be reflected in changes to the peak positions in the X-ray diffraction patterns, since Li-ions are preferentially inserted and stored in the van der Waals gap of the material.

As mentioned earlier, first-order phase transitions are not suppressed in $bMoS_2$ during lithiation. Figure 4a shows the diffraction pattern of $bMoS_2$ upon cycling at 0.22 C. During lithiation of $bMoS_2$, the (001) peak first shifts toward lower Q values. This is then followed by a shift to higher Q at a voltage of ~1.76 V and is accompanied by the appearance of an additional peak at 1.09 $Å^{-1}$ that grows continuously in intensity as the Li-ion concentration increases. During delithiation, the structural processes that occurred during lithiation are reversible. The peak at 1.09 $Å^{-1}$ disappears, while

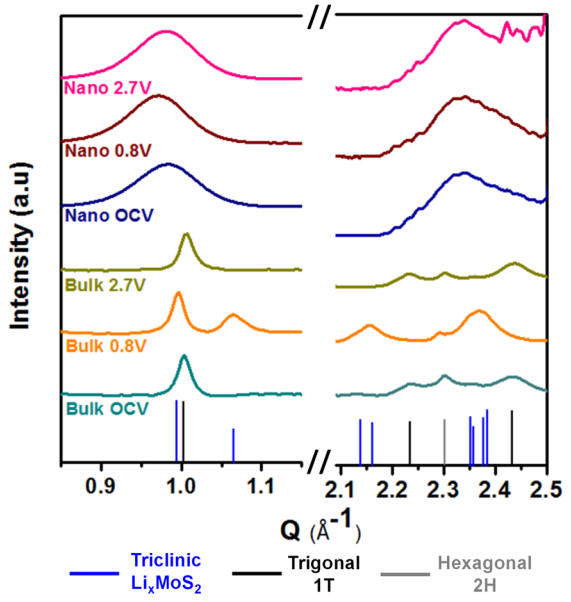

Figure 5. Selected XRD patterns for the pristine, lithiated and delithiated states of $bMoS_2$ and $nMoS_2$ with line patterns of the three known phases of MoS_2. This direct comparison indicates that $bMoS_2$ experiences major phase transitions between the 1T trigonal prismatic phase to the triclinic $Li1MoS_2$ phase, which has also been observed in the literature. However, this phase transition is not observed in $nMoS_2$. Shoulders and peaks corresponding to the triclinic $LiMoS_2$ phase are clearly absent in the $nMoS_2$ at 0.8 V (all voltages reported versus Li/Li^+).

the (001) peak gradually returns to its original position. In addition to this change, significant structural changes corresponding to rearrangement of the covalent network in the MoS_2 layers can also be found in the region between 2.1 $Å^{-1}$ and 2.5 $Å^{-1}$. Similar to the (001) peak, the (100) and (101) peaks shift significantly toward lower Q, and the (101) peak merges with its shoulder peak during lithiation and then moves back to higher Q during delithiation. These diffraction signatures are consistent with a reversible first-order phase change, which typically occurs when Li-ions have a low solubility in the parent phase (the 1T-metallic phase in this case).

Very different structural changes are found in $nMoS_2$ compared to $bMoS_2$ during Li-ion charge storage. Figure 4b shows the XRD patterns of $nMoS_2$ collected during the *operando* phase change study at 0.22 C. As seen in Figure 4b, all (001), (100), and (101) peaks shift to lower Q (0.013 $Å^{-1}$) without the emergence of any additional peaks (the distinct shoulder at 1.09 $Å^{-1}$ is not present) during lithium intercalation and deintercalation of $nMoS_2$, indicating the suppression of phase transition. It is also worth noting that unlike $bMoS_2$, the expansion of $nMoS_2$ lattice tracks the Li-ion concentration linearly, like a solid solution. This lattice expansion indicates that the fast charge storage in this system is not limited to the surface of the nanocrystal and is indeed related to the fact that a large portion (80%) of the theoretical capacity being stored through capacitive mechanisms in a process that can best be described as intercalation pseudocapacitance.[57]

To further emphasize this point, three known MoS_2 phases, 2H, 1T, and triclinic Li_1MoS_2, were compared to the diffraction patterns for $bMoS_2$ and $nMoS_2$ in different states of charge. Figure 5 shows the diffraction line pattern of the

DOI: 10.1021/acsnano.8b06381
ACS Nano 2019, 13, 1223−1231

hexagonal (2H), trigonal prismatic (1T), and triclinic phases and the synchrotron based XRD pattern of the pristine, lithiated and delithiated states of $bMoS_2$ and $nMoS_2$. Prior to the *operando* study cycling (after 2H-1T conversion precycling), $bMoS_2$ consists mainly of the expected trigonal prismatic 1T phase with some residual hexagonal 2H phase. The back conversion of the 1T-2H phase is known to occur slowly at room temperature in the fully delithiated state and probably happened during the 24-h transit period before the samples were analyzed.[43] The Li_1MoS_2, which is a distinctly different phase than the 1T phase, matches the triclinic MoS_2 powder pattern indicating that $bMoS_2$ undergoes a first-order phase change upon Li-ion intercalation.[58] The full reversibility of this phase transformation can be seen from the diffraction patterns as the delithiated MoS_2 returns to the trigonal phase, this time with reduced hexagonal phase content. By contrast, distinct changes in the XRD patterns are not observed in $nMoS_2$. If phase changes were to occur in $nMoS_2$, even with peak broadening due to finite size effects, a shoulder should have appeared on the (001) peak and an additional peak should appear at 2.1 $Å^{-1}$ in the covalent region, indicating the presence of the triclinic Li_1MoS_2 phase. The absence of those peaks confirms phase transition suppression in $nMoS_2$ and confirms that intercalation in $nMoS_2$ nanocrystals is pseudocapacitive. As mentioned earlier, only a peak shift to lower Q is observed during lithiation as a result of lattice expansion. We note that the $nMoS_2$ peaks are already shifted to lower Q to begin with due to a larger than standard van der Waals gap (6.27 Å versus 6.15 Å in bulk). Interesting, this expansion does not affect the changes in peak position observed during charge and discharge.

We speculate that the difference in structural changes between the bulk and the nano could be related to kinetic barrier.[59] The phase transition found in $bMoS_2$ could be suppressed in the nanoscale material if the formation of stable nuclei in a confined space was energetically unfavorable. Even if such nuclei were formed, the formation of a phase boundary interface would incur a significant free energy penalty.[51,52,60] Thus, two-phase coexistence could be inhibited in nanocrystals due to the limited crystallite size. The fact that each nucleation event can only transform one crystallite could also result in phase transition suppression and the accompanying fast insertion kinetics. We also postulate that the miscibility gap could be reduced in $nMoS_2$, either because of the increased van der Waal's gap or because of increased surface energy contribution to the overall system energy.

CONCLUSIONS

In order to better understand differences in charge storage mechanisms for $bMoS_2$ and $nMoS_2$, we have investigated the structural changes and phase stability that occur during the lithiation and delithiation of both bulk and nano MoS_2. We have correlated the disparate electrochemistry of these two samples with structural information obtained from synchrotron-based *operando* X-ray diffraction upon electrochemical cycling. The galvanostatic voltage profiles of $bMoS_2$ and $nMoS_2$ electrodes show discrete plateaus and linear voltage responses, respectively. This behavior, along with the fast kinetics and low polarization observed in $nMoS_2$, suggests battery-like behavior in the bulk material and pseudocapacitive behavior in the nanoscale system. In agreement with this observation, $bMoS_2$ shows a first-order phase change between the trigonal to triclinic phase as Li ions insert into the host lattice. By contrast, $nMoS_2$ shows no change other than a small shift in lattice constant. This indicates that the pseudocapacitive behavior of $nMoS_2$ is mostly due to a suppressed first-order phase transition that occurs in the 1T phase, in a process that can best be described as intercalation pseudocapacitance. These results help explain the very fast cycling kinetics that has been demonstrated for nanostructured MoS_2.

Perhaps more importantly, this work adds another concrete realization to the hypothesis that intercalation pseudocapacitance can occur when ion-intercalation is not accompanied by a phase transition. Some past studies have demonstrated this correlation in materials that are intrinsically able to intercalate Li^+ with minimal structural change.[4] Such materials have been termed intrinsic pseudocapacitors.[61] In this case, however, materials that show standard battery behavior in the bulk are converted to a pseudocapacitor in finite size, and that conversion is accompanied by suppression of the standard intercalation induced phase transition. Such materials have been termed extrinsic pseudocapacitors,[61] and this family of materials is potentially very large and thus very interesting for future energy storage applications. By directly correlating the altered electrochemical kinetics with suppression of phase transitions in finite sized materials, we strengthen this correlation and hopefully add insight that will lead to the future development of pseudocapacitive nanostructured materials.

METHODS

Synthesis. All starting materials were obtained from commercial suppliers and used without further purification. Bulk MoS_2 was purchased from Alfa Aesar. The MoS_2 nanocrystals were synthesized through sulfurization of nanosized MoO_2. The synthesis of MoO_2 nanocrystals has been reported elsewhere[12] and is briefly described here. The MoS_2 nanocrystals were synthesized through sulfurization of nanosized MoO_2. The nanosized-MoO_2 was prepared in a 45 mL Teflon liner by dissolving 270 mg of anhydrous $MoCl_5$ (Strem Chemicals) in a mixture of 5 mL of ethanol and 15 mL of deionized water at a reaction temperature of 180 °C for 6 h. The MoO_2 nanocrystals were converted to MoS_2 with H_2S gas. The reaction was carried out in a tube furnace at 600 °C under flowing H_2S/H_2 (H_2S 5 mol %: H_2 95 mol %, Air Gas) for 10 h. A graphite boat was used to convert ≈100−200 mg of MoO_2 to MoS_2 in each synthetic run.[27]

Characterization. Powder X-ray diffraction (XRD) was performed on a PANalytical X'Pert Pro operating with Cu K_α (λ = 1.5418 Å) using a 0.03° step size, a voltage of 45 kV, and a current of 40 mA to characterize the pristine $nMoS_2$ diffraction. XRD patterns were recorded in the range of $10° < 2\theta < 80°$. Transmission electron microscopy (TEM) was performed using a FEI Technai T12 operating at 120 kV. *Operando* XRD was performed at SSRL at beamline 11-3 at an X-ray energy of 12300 eV. *Operando* data was collected using a MAR 345 Image Plate with 130 mm work distance. Data was collected from Q = 0 to 5.5 $Å^{-1}$.

Electrochemistry. Carbon-based slurry electrodes were made and used for all electrochemical cycling. Electrodes have an overall composition of 70 wt % active material ($nMoS_2$ or $bMoS_2$):10 wt % vapor grown carbon fibers (Sigma-Aldrich):10 wt % carbon black (Alfa Aesar):10 wt % polyvinylidene fluoride (Kynar) binder, all dispersed in *N*-methyl-2-pyrrolidone (Alpha Aesar). All components were mixed in a mortar and pestle to obtain a homogeneous paste and cast onto a 25 μm carbon-coated aluminum current collector. The slurry was dried in ambient temperature for 5 h prior to drying in a vacuum oven for 15 h at 125 °C. The mass loading of the electrodes was 3.42 mg cm^{-2} and 5.82 mg cm^{-2} for $bMoS_2$ and $nMoS_2$, respectively. These electrodes were cycled from 1.0 to 2.7 V in Swagelok cells using lithium metal counter electrodes, glass fiber separator (Watman), and 1 M $LiPF_6$ electrolyte in 1 ethylene carbonate:1 diethylene carbonate by volume (Sigma). $nMoS_2$ samples

DOI: 10.1021/acsnano.8b06381
ACS Nano 2019, 13, 1223−1231

were cycled using VSP potentiostat/galvanostat (Bio-Logic) at a 0.2 C rate (138.6 mA h g^{-1}), while the $bMoS_2$ electrodes were cycled on Arbin using at a 0.2 C rate (50 mA h g^{-1}).

After precycling, the electrodes were taken out of the Swagelok cells in an Ar-filled glovebox and reassembled into in a coin cell with 3 mm holes and Kapton tape windows for the *operando* studies. The Kapton tape window was chosen for X-ray transparency. The coin cells were stored in an Ar atmosphere until cycling was performed to prevent exposure. Due to time constraints, all cycling was performed at 0.22 C for the *operando* studies at SSRL.

Data Processing. All diffraction intensity data is plotted as a function of the scattering vector length $Q = \frac{4\pi}{\lambda}\sin(\theta)$, where θ is half of the scattering angle, and λ = is the wavelength of the incident radiation; the *d*-spacing thus is simply $\frac{2\pi}{Q}$.

All diffraction peaks were normalized to the Al peak using an Area Diffraction Machine. Background subtraction of all spectra was later performed in Origin. Diffraction of a blank cell (a regular coin cell with a Kapton window containing all components except the active material) was used as the background diffraction pattern.

ASSOCIATED CONTENT

Supporting Information

The Supporting Information is available free of charge on the ACS Publications website at DOI: 10.1021/acsnano.8b06381.

TEM images of the MoS_2 nanocrystals used in this study and nanocrystal size distribution calculated from those images (PDF)

AUTHOR INFORMATION

Corresponding Author

*E-mail: tolbert@chem.ucla.edu.

ORCID

Bruce S. Dunn: 0000-0001-5669-4740

Sarah H. Tolbert: 0000-0001-9969-1582

Present Addresses

[⊥]Xerion Advanced Battery Corporation, 3100 Research Boulevard St. 320, Kettering, OH 45420, U.S.A.

[#]Center of Energy Storage Research, Korea Institute of Science and Technology, Hwarang-ro 14-gil 5, Seongbuk-gu, Seoul 136-791, Republic of Korea.

[∥]Applied Materials Inc., 3050 Bowers Avenue, Santa Clara, California 95054, U.S.A.

Author Contributions

J.B.C. and T.C.L. contributed to the work equally. J.B.C., T.C.L., and S.H.T conceived and planned the experiment. J.B.C. and T.C.L. prepared electrodes, characterized materials, performed electrochemical studies, assembled *operando* cells, and carried out the *operando* X-ray diffraction measurements. J.B.C., T.C.L., and S.H.T. performed the diffraction analysis and interpretation. J.B.C., H.K., and A.S. developed and prepared the MoO_2 and MoS_2 nanocrystals.

Notes

The authors declare no competing financial interest.

ACKNOWLEDGMENTS

This work was supported by the US Department of Energy, Office of Science, Office of Basic Energy Sciences under Award Number DE-SC0014213. Use of the Stanford Synchrotron Radiation Lightsource, SLAC National Accelerator Laboratory, is supported by the U.S. Department of Energy, Office of Science, Office of Basic Energy Sciences under Contract No. DE-AC02-76SF00515.

REFERENCES

(1) Augustyn, V.; Simon, P.; Dunn, B. Pseudocapacitive Oxide Materials for High-Rate Electrochemical Energy Storage. *Energy Environ. Sci.* **2014**, *7*, 1597−1614.

(2) Cook, J. B.; Kim, H.; Yan, Y.; Ko, J. S.; Robbennolt, S.; Dunn, B.; Tolbert, S. H. Mesoporous MoS2 as a Transition Metal Dichalcogenide Exhibiting Pseudocapacitive Li and Na-Ion Charge Storage. *Adv. Energy Mater.* **2016**, *6*, 1501937.

(3) Zhu, Y.; Peng, L.; Chen, D.; Yu, G. Intercalation Pseudocapacitance in Ultrathin $VOPO_4$ Nanosheets: Toward High-Rate Alkali-Ion-Based Electrochemical Energy Storage. *Nano Lett.* **2016**, *16*, 742−747.

(4) Augustyn, V.; Come, J.; Lowe, M. A.; Kim, J. W.; Taberna, P.; Tolbert, S. H.; Abruña, H. D.; Simon, P.; Dunn, B. High-Rate Electrochemical Energy Storage through Li+ Intercalation Pseudocapacitance. *Nat. Mater.* **2013**, *12*, 518−522.

(5) Conway, B. E.; Pell, W. G. Double-Layer and Pseudocapacitance Types of Electrochemical Capacitors and Their Applications to the Development of Hybrid Devices. *J. Solid State Electrochem.* **2003**, *7*, 637−644.

(6) Li, D.; Zhou, H. Two-Phase Transition of Li-Intercalation Compounds in Li-Ion Batteries. *Mater. Today* **2014**, *17*, 451−463.

(7) Van Der Ven, A.; Garikipati, K.; Kim, S.; Wagemaker, M. The Role of Coherency Strains on Phase Stability in LiXFePO4: Needle Crystallites Minimize Coherency Strain and Overpotential. *J. Electrochem. Soc.* **2009**, *156*, A949−A957.

(8) Van Der Ven, A.; Bhattacharya, J.; Belak, A. A. Understanding Li Diffusion in Li- Intercalation Compounds. *Acc. Chem. Res.* **2013**, *46*, 1216−1225.

(9) Zheng, J. P.; Cygan, P. J.; Jow, T. R. Hydrous Ruthenium Oxide as an Electrode Material for Electrochemical Capacitors. *J. Electrochem. Soc.* **1995**, *142*, 2699−2703.

(10) Lee, H. Y.; Goodenough, J. B. Supercapacitor Behavior with KCl Electrolyte. *J. Solid State Chem.* **1999**, *144*, 220−223.

(11) Brousse, T.; Toupin, M.; Dugas, R.; Athouël, L.; Crosnier, O.; Bélanger, D. Crystalline MnO_2 as Possible Alternatives to Amorphous Compounds in Electrochemical Supercapacitors. *J. Electrochem. Soc.* **2006**, *153*, A2171−A2180.

(12) Kim, H.; Cook, J. B.; Tolbert, S. H.; Dunn, B. The Development of Pseudocapacitive Properties in Nanosized-MoO_2. *J. Electrochem. Soc.* **2015**, *162*, A5083−A5090.

(13) Van De Krol, R.; Goossens, A.; Meulenkamp, E. A. *In Situ* X-Ray Diffraction of Lithium Intercalation in Nanostructured and Thin Film Anatase TiO_2. *J. Electrochem. Soc.* **1999**, *146*, 3150−3154.

(14) Brezesinski, T.; Wang, J.; Polleux, J.; Dunn, B.; Tolbert, S. H. Templated Nanocrystal-Based Porous TiO_2 Films for Next-Generation Electrochemical Capacitors. *J. Am. Chem. Soc.* **2009**, *131*, 1802−1809.

(15) Wang, J.; Polleux, J.; Lim, J.; Dunn, B. Pseudocapacitive Contributions to Electrochemical Energy Storage in TiO_2 (Anatase) Nanoparticles. *J. Phys. Chem. C* **2007**, *111*, 14925−14931.

(16) Muller, G. A.; Cook, J. B.; Kim, H.; Tolbert, S. H.; Dunn, B. High Performance Pseudocapacitor Based on 2D Layered Metal Chalcogenide Nanocrystals. *Nano Lett.* **2015**, *15*, 1911−1917.

(17) Lesel, B. K.; Ko, J. S.; Dunn, B.; Tolbert, S. H. Mesoporous $LixMn_2O_4$ Thin Film Cathodes for Lithium-Ion Pseudocapacitors. *ACS Nano* **2016**, *10*, 7572−7581.

(18) Lesel, B. K.; Cook, J. B.; Yan, T.; Lin, T. C.; Tolbert, S. H. Using Nanoscale Domain Size To Control Charge Storage Kinetics in Pseudocapacitive Nanoporous $LiMn_2O_4$ Powders. *ACS Energy Lett.* **2017**, *2*, 2293−2298.

(19) Balke, N.; Jesse, S.; Morozovska, A. N.; Eliseev, E.; Chung, D. W.; Kim, Y.; Adamczyk, L.; Garcia, R. E.; Dudney, N.; Kalinin, S. V. Nanoscale Mapping of Ion Diffusion in a Lithium-Ion Battery Cathode. *Nat. Nanotechnol.* **2010**, *5*, 749−754.

(20) Zhang, X.; Van Hulzen, M.; Singh, D. P.; Brownrigg, A.; Wright, J. P.; Van Dijk, N. H.; Wagemaker, M. Rate-Induced Solubility and Suppression of the First-Order Phase Transition in Olivine $LiFePO_4$. *Nano Lett.* **2014**, *14*, 2279−2285.

DOI: 10.1021/acsnano.8b06381
ACS Nano 2019, 13, 1223−1231

(21) Brezesinski, T.; Wang, J.; Tolbert, S. H.; Dunn, B. Ordered Mesoporous α-MoO_3 with Iso-Oriented Nanocrystalline Walls for Thin-Film Pseudocapacitors. *Nat. Mater.* **2010**, *9*, 146−151.
(22) Acerce, M.; Voiry, D.; Chhowalla, M. Metallic 1T Phase MoS_2 Nanosheets as Supercapacitor Electrode Materials. *Nat. Nanotechnol.* **2015**, *10*, 313−318.
(23) Stephenson, T.; Li, Z.; Olsen, B.; Mitlin, D. Lithium Ion Battery Applications of Molybdenum Disulfide (MoS_2) Nanocomposites. *Energy Environ. Sci.* **2014**, *7*, 209−231.
(24) Pandey, M.; Bothra, P.; Pati, S. K. Phase Transition of MoS_2 Bilayer Structures. *J. Phys. Chem. C* **2016**, *120*, 3776−3780.
(25) Zhang, R.; Tsai, I.; Chapman, J.; Khestanova, E.; Waters, J.; Grigorieva, I. V. Superconductivity in Potassium-Doped Metallic Polymorphs of MoS_2. *Nano Lett.* **2016**, *16*, 629−636.
(26) Huang, Q.; Li, X.; Sun, M.; Zhang, L.; Song, C.; Zhu, L.; Chen, P.; Xu, Z.; Wang, W.; Bai, X. The Mechanistic Insights into the 2H-1T Phase Transition of MoS_2 upon Alkali Metal Intercalation: From the Study of Dynamic Sodiation Processes of MoS_2 Nanosheets. *Adv. Mater. Interfaces* **2017**, *4*, 1700171.
(27) Cook, J. B.; Kim, H.; Lin, T. C.; Lai, C.; Dunn, B.; Tolbert, S. H. Pseudocapacitive Charge Storage in Thick Composite MoS_2 Nanocrystal-Based Electrodes. *Adv. Energy Mater.* **2017**, *7*, 1601283.
(28) Reimers, J. N.; Dahn, J. R. Electrochemical and *In Situ* X-Ray Diffraction Studies of Lithium Intercalation in Li_xCoO_2. *J. Electrochem. Soc.* **1992**, *139*, 2091−2096.
(29) Mukerjee, S.; Thurston, R.; Jisrawi, N. M.; Yang, X.; Mcbreen, J. Structural Evolution of $Li_xMn_2O_4$ in Lithium-Ion Battery Cells Measured *In Situ* Using Synchrotron X-Ray Diffraction Techniques. *J. Electrochem. Soc.* **1998**, *145*, 466−472.
(30) Li, W.; Reimers, J. N.; Dahn, J. R. *In Situ* X-Ray Diffraction and Electrochemical Studies of Li1-xNiO2. *Solid State Ionics* **1993**, *67*, 123−130.
(31) Yoo, H.; Tiwari, A. P.; Lee, J.; Kim, D.; Park, J. H.; Lee, H. Cylindrical Nnostructured MoS2 Directly Grown on CNT Composites for Lithium-Ion Batteries. *Nanoscale* **2015**, *7*, 3404−3409.
(32) Teng, Y.; Zhao, H.; Zhang, Z.; Li, Z.; Xia, Q.; Zhang, Y.; Zhao, L.; Du, X.; Du, Z.; Lv, P.; Swierczek, K. MoS2 Nanosheets Vertically Grown on Graphene Sheets for Lithium-Ion Battery Anodes. *ACS Nano* **2016**, *10*, 8526−8535.
(33) Hwang, H.; Kim, H.; Cho, J. MoS2 Nanoplates Consisting of Disordered Graphene-like Layers for High Rate Lithium Battery Anode Materials. *Nano Lett.* **2011**, *11*, 4826−4830.
(34) Deng, Z.; Jiang, H.; Hu, Y.; Liu, Y.; Zhang, L.; Liu, H.; Li, C. 3D Ordered Macroporous MoS2@C Nanostructure for Flexible Li-Ion Batteries. *Adv. Mater.* **2017**, *29*, 1603020.
(35) Jiao, Y.; Mukhopadhyay, A.; Ma, Y.; Yang, L.; Hafez, A. M.; Zhu, H. Ion Transport Nanotube Assembled with Vertically Aligned Metallic MoS2 for High Rate Lithium-Ion Batteries. *Adv. Energy Mater.* **2018**, *8*, 1702779.
(36) Wei, Q.; Gao, M.-R.; Li, Y.; Zhang, D.; Wu, S.; Chen, Z.; Sun, Y. Directionally Assembled MoS2 with Significantly Expanded Interlayer Spacing: A Superior Anode Material for High-Rate Lithium-Ion Batteries. *Mater. Chem. Front.* **2018**, *2*, 1441−1448.
(37) Laman, F. C.; Brandt, K. Effect of Discharge Current on Cycle Life of a Rechargeable Lithium Battery. *J. Power Sources* **1988**, *24*, 195−206.
(38) Fang, X.; Hua, C.; Guo, X.; Hu, Y.; Wang, Z.; Gao, X.; Wu, F.; Wang, J.; Chen, L. Lithium Storage in Commercial MoS2 in Different Potential Ranges. *Electrochim. Acta* **2012**, *81*, 155−160.
(39) Wang, H.; Lu, Z.; Xu, S.; Kong, D.; Cha, J. J.; Zheng, G.; Hsu, P.; Yan, K. Electrochemical Tuning of Vertically Aligned MoS2 Nano Films and Its Application in Improving Hydrogen Evolution Reaction. *Proc. Natl. Acad. Sci. U. S. A.* **2013**, *110*, 19701−19706.
(40) Wang, X.; Shen, X.; Wang, Z.; Yu, R.; Chen, L. Atomic-Scale Clarification of Structural Transition of MoS2 upon Sodium Intercalation. *ACS Nano* **2014**, *8*, 11394−11400.
(41) Wang, L.; Xu, Z.; Wang, W.; Bai, X. Atomic Mechanism of Dynamic Electrochemical Lithiation Processes of MoS2 Nanosheets. *J. Am. Chem. Soc.* **2014**, *136*, 6693−6697.
(42) Lin, Y.; Dumcenco, D. O.; Huang, Y.; Suenaga, K. Atomic Mechanism of the Semiconducting to Metallic Phase Transition in Single-Layered MoS2. *Nat. Nanotechnol.* **2014**, *9*, 391−396.
(43) Py, A.; Haering, R. R. Structural Destabilization Induced by Lithium Intercalation in MoS2 and Related Compounds. *Can. J. Phys.* **1983**, *61*, 76−84.
(44) Imanishi, N.; Toyoda, M.; Takeda, Y.; Yamamoto, O. Study on Lithium Intercalation into MoS2. *Solid State Ionics* **1992**, *58*, 333−338.
(45) Voiry, D.; Mohite, A.; Chhowalla, M. Phase Engineering of Transition MetalDichalcogenides. *Chem. Soc. Rev.* **2015**, *44*, 2702−2712.
(46) Xiong, F.; Wang, H.; Liu, X.; Sun, J.; Brongersma, M.; Pop, E.; Cui, Y. Li Intercalation in MoS2: *In Situ* Observation of Its Dynamics and Tuning Optical and Electrical Properties. *Nano Lett.* **2015**, *15*, 6777−6784.
(47) Wypych, F.; Schollhorn, R. 1T-MoS2, a New Metallic Modification of Molybdenum Disulfide. *J. Chem. Soc., Chem. Commun.* **1992**, *0*, 1386−1388.
(48) Mulhern, P. J. Lithium Intercalation in Crystalline LixMoS2. *Can. J. Phys.* **1989**, *67*, 1049−1052.
(49) Gao, P.; Wang, L.; Zhang, Y.; Huang, Y.; Liu, K. Atomic-Scale Probing of the Dynamics of Sodium Transport and Intercalation-Induced Phase Transformations in MoS2. *ACS Nano* **2015**, *9*, 11296−11301.
(50) Guo, Y.; Sun, D.; Ouyang, B.; Raja, A.; Song, J.; Heinz, T. F.; Brus, L. E. Probing the Dynamics of the Metallic-to-Semiconducting Structural Phase Transformation in MoS2 Crystals. *Nano Lett.* **2015**, *15*, 5081−5088.
(51) Tolbert, S. H.; Alivisatos, A. P. The Wurtzite to Rock Salt Structural Transformation in CdSe Nanocrystals under High Pressure. *J. Chem. Phys.* **1995**, *102*, 4642−4656.
(52) Tolbert, S. H.; Alivisatos, A. P. Size Dependence of a First Order Solid-Solid Phase Transition The Wurtzite to Rock Salt Transformation in CdSe Nanocrystals. *Science* **1994**, *265*, 373−376.
(53) Van Der Ven, A.; Wagemaker, M. Effect of Surface Energies and Nano-Particle Size Distribution on Open Circuit Voltage of Li-Electrodes. *Electrochem. Commun.* **2009**, *11*, 881−884.
(54) Li, H.; Zhu, Y.; Dong, S.; Shen, L.; Chen, Z.; Zhang, X.; Yu, G. Self-Assembled Nb2O5 Nanosheets for High Energy-High Power Sodium Ion Capacitors. *Chem. Mater.* **2016**, *28*, 5753−5760.
(55) Rauda, I. E.; Augustyn, V.; Saldarriaga-lopez, L. C.; Chen, X.; Schelhas, L. T.; Rubloff, G. W.; Dunn, B.; Tolbert, S. H. Nanostructured Pseudocapacitors Based on Atomic Layer Deposition of V2O5 onto Conductive Nanocrystal-Based Mesoporous ITO Scaffolds. *Adv. Funct. Mater.* **2014**, *24*, 6717−6728.
(56) Xiao, X.; Peng, Z.; Chen, C.; Zhang, C.; Beidaghi, M.; Yang, Z.; Wu, N.; Huang, Y.; Miao, L.; Gogotsi, Y.; Zhou, J. Freestanding MoO3-x Nanobelt/Carbon Nanotube Films for Li-Ion Intercalation Pseudocapacitors. *Nano Energy* **2014**, *9*, 355−363.
(57) Huggins, R. A. Supercapacitors and Electrochemical Pulse Sources. *Solid State Ionics* **2000**, *134*, 179−195.
(58) Reshak, A. H.; Auluck, S. Calculated Optical Properties of 2H-MoS2 Intercalated with Lithium. *Phys. Rev. B: Condens. Matter Mater. Phys.* **2003**, *68*, 125101.
(59) Brus, L. E.; Harkless, J. A. W.; Stillinger, F. H. Theoretical Metastability of Semiconductor Crystallites in High-Pressure Phases, with Application to β-Tin Structure Silicon. *J. Am. Chem. Soc.* **1996**, *118*, 4834−4838.
(60) Wagemaker, B. M.; Mulder, F. M.; Van Der Ven, A. The Role of Surface and Interface Energy on Phase Stability of Nanosized Insertion Compounds. *Adv. Mater.* **2009**, *21*, 2703−2709.
(61) Simon, P.; Gogotsi, Y.; Dunn, B. Where Do Batteries End and Supercapacitors Begin? *Science* **2014**, *343*, 1210−1211.

DOI: 10.1021/acsnano.8b06381
ACS Nano 2019, 13, 1223−1231